

# Synthesis and Characterization of Porous Sulfur/MWCNTs Composites with Improved Performance and Safety as Cathodes for Li-S Batteries

Andrea Strakova Fedorkova<sup>1,\*</sup>, Tomas Kazda<sup>2</sup>, Katarina Gavalierova<sup>1</sup>, Pedro Gomez-Romero<sup>3</sup>, Elena Shembel<sup>4</sup>

<sup>1</sup> Institute of Chemistry, Faculty of Science, P.J. Šafárik University, Moyzesova 11, 041 54 Košice, Slovakia

<sup>2</sup> Department of Electrical and Electronic Technology, Faculty of Electrical Engineering and Communication, Brno University of Technology, Technická 10, 616 00 Brno, Czech Republic

<sup>3</sup> Institut Català de Nanociència i Nanotecnologia, ICN2, CIN2 / Consejo Superior de Investigaciones Científicas (CSIC), Campus UAB, E-08193 Bellaterra, Barcelona, Spain

<sup>4</sup> Ukrainian State University of Chemical Technology, Gagarin Ave. 8, Dnipropetrovsk, Ukraine, 49005

\*E-mail: [andrea.fedorkova@upjs.sk](mailto:andrea.fedorkova@upjs.sk)

Received: 30 September 2017 / Accepted: 24 November 2017 / Published: 16 December 2017

---

Sulfur-carbon (S-C-MWCNTs) composites and sulfur-LiFePO<sub>4</sub> (S-LFP-MWCNTs) composites were synthesised with MWCNTs additive by sulfur sublimation and solid state reaction. As prepared materials are characterized with scanning electron microscopy, thermogravimetry, FTIR, elemental analysis, XPS, cyclic voltammetry and galvanostatic charge/discharge tests. The composite S-LFP cathode with MWCNTs additive shows improved discharge capacity and performance. It shows an initial discharge capacity of 1167 mAh/g-sulfur, or 70% of theoretical capacity. The discharge capacity measured after 20 cycles for S-LFP-MWCNTs composite cathode was 80% of the initial capacity and remained stable. After 160 charge/discharge tests, the cathode displays a stable capacity of 561 mAh/g-sulfur at the C-rate of 0.2 C. Combination of sulfur, LiFePO<sub>4</sub> and MWCNTs prevents aggregation and volume change of the cathode particles and improves the conductivity and electrochemical stability during the long-term cycling. 3-D FTIR spectroscopy measurements confirmed improved chemical stability and safety of sulfur composites also at higher temperatures.

---

**Keywords:** Sulfur composite cathode, Lithium batteries, LiFePO<sub>4</sub>, multi-wall carbon nanotubes

## 1. INTRODUCTION

State of the art Li-ion batteries used in Electric Vehicles (EVs) currently provide a driving range up to 150 km on a single charge and more than half of the total price of the vehicle is cost of the

battery. The lithium-sulfur battery is presently being reconsidered as a good candidate to reach both goals upon further improvement. Conventional Li-ion batteries are based on intercalation process while Li-S batteries are the conversion type. During the charge and discharge procedure electrochemical reactions occurs and new chemical compounds are produced [1-3]. Sulfur is the active cathode material with a theoretical capacity of 1672 mAh/g and an average discharge potential of 2.2 V versus lithium. Energy density up to 500 Wh/kg could be achieved for Li-S batteries and this value is three times higher than for classical intercalation batteries [4].

The advantage of lithium-sulfur batteries is high capacity, low price, environmental compatibility and high energy density. The biggest problem of the sulfur cathode is its poor cyclability and life-time stability. Intermediate polysulfide ions are created during the discharge process of sulfur cathodes. Higher polysulfides are easily dissolved in the electrolyte during the charge/discharge reactions and sulfur active material is lost during the cycling [3,5,6]. Our research will be focused on the most important challenges in the field of Li-S batteries as polysulfide dissolution, volume expansion, self-discharge or insulating active material sulfur.

Sulfur cathode performance can be improved using a several combinations of sulfur with conductive materials, such as creating a sulfur-carbon composites with carbon black, MWCNTs or nanostructured carbon that have resulted in much improved characteristics [7–13]. Conductive polymers [14,15], activated carbons [16], and multi-walled carbon nanotubes [10,13,17] have been reported as absorbing agents in lithium/sulfur batteries thanks to their strong absorbing properties to the polysulfides and high electronic conductivity. Conducting polymer polypyrrole with high porosity has also great absorbing ability to the sulfur and polysulfides. This polymer can also retard solubility of higher polysulfides [18-20].

In this research paper, we combine LFP, carbon, MWCNTs and sublimed sulfur to a simple to create S-C and S-LFP cathode material with MWCNTs additive with high porosity. Scanning electron microscopy (SEM), thermogravimetry (TGA), X-ray photoelectron spectroscopy (XPS), 3-D FTIR spectroscopy, cyclic voltammetry (CV) and charge-discharge measurements of the S-C and S-LFP composites with MWCNTs were used for characterization of our electrodes.

## 2. EXPERIMENTAL

### 2.1. Preparation of sulfur composites

Sulfur-carbon composite was synthesized by heating the mixture of sulfur (Sigma-Aldrich) and carbon Super P (Timcal) at 150 °C for 15 minutes. Sulfur at this temperature has low viscosity and can penetrate into the pores of carbon black. The weight ratio of Super P:S was 1:2. The sulfur content in the S-C composite measured by TG-DSC was about 48 wt%.

Sulfur-LFP composite was synthesised by a solid state reaction in planetary ball mill. Sulfur (Sigma-Aldrich) and LiFePO<sub>4</sub> (preparation technique described in [15]) were placed into the jar with a ratio of 70:30 and milled for 30 min at 800 rpm with MWCNTs additive (5 wt. %).

## 2.2. Preparation of cathodes and test cells

Electrode slurries were made by mixing the sulfur composite as the active material with polyvinylidene fluorid (PVdF) in N-methyl-2-pyrrolidone (NMP) with a weight ratio of 80:20. The slurry was then coated onto aluminium foil as current collector using the doctor-blade technique. All samples were dried in a vacuum oven at 120 °C for 18 h. Round electrodes with 18 mm diameter were cut out of the coated foil, with an area of 2.54 cm<sup>2</sup> and total mass of 1.5–2 mg on a substrate of Al foil. Test cells (El-cell®) were assembled in an Ar-filled glove box (Jacomex) with the lithium metal as the counter electrode and lithium metal as the reference electrode, and the glass fibre separator. The electrolyte was 0.7 M lithium bis(tri fluoromethanesulfone)imide (LiTFSI) dissolved in a solvent mixture of DME and DIOX (2:1) with 0.25 M LiNO<sub>3</sub> as an additive.

## 2.3. Sample characterization

Scanning electron microscope Quanta 200 ESEM FEG and JEOL JSM-7000F + EDX INCA were used to observe the structure and morphology of samples.

Thermogravimetric experiments and the evolutionary FT-IR profiles of scales were collected on a TG-DTA analyzer SDT Q600 (Thermal instruments). 20 mg of sample was inserted into platinum cup and heated up to 600 °C (heating rate was 5 °C/min).

X-ray photoelectron spectroscopy (XPS) data were obtained on a Microlab350 using a Spherical Sector Analyser. The X-ray source was a nonmonochromated MgK $\alpha$  line ( $E = 1253.6$  eV) working at 300 W and the spot size was  $5 \times 2$  mm<sup>2</sup>. Survey and multi region spectra of C 1s, O 1s and N 1s were acquired at high energy resolution (pass energy of 20 eV) to perform quantification and peak fitting.

Charge/discharge and cyclic voltammetry measurements were performed with BioLogic potentiostat in voltage range between 1.8 and 2.8 V vs. Li<sup>+</sup>/Li at room temperature. A typical sulfur mass loading on the electrode was 0.8–0.9 mg/cm<sup>2</sup>.

## 3. RESULTS AND DISCUSSION

The surface structure and morphology of the sulfur-based composite electrodes were investigated by SEM and are shown in Fig 1. Two different structures were observed for S-C composite. Figures 1a,b present the structure of the sulfur-carbon composite. The surface of the Sulfur-Carbon sample (Figure 1a) is homogeneous without any significant cracks or holes. The overall structure is porous enough for transport of Li<sup>+</sup> ions and electrolyte infiltration.

The structure of S-C-MWCNTs sample (Figure 1b) is somewhat different. The porous and homogeneous basis is saved but MWCNTs additive induced the formation of larger pores and holes. The MWCNTs are also clearly visible and provide the connections between S and C. This network structure is providing excellent pathways for electrons into the structure containing insulating sulfur. High porosity of samples created by close contact between the carbon, sulfur and MWCNTs is creating

also many adsorbent points on the surface of active material to avoid the loss of the soluble higher polysulfides.

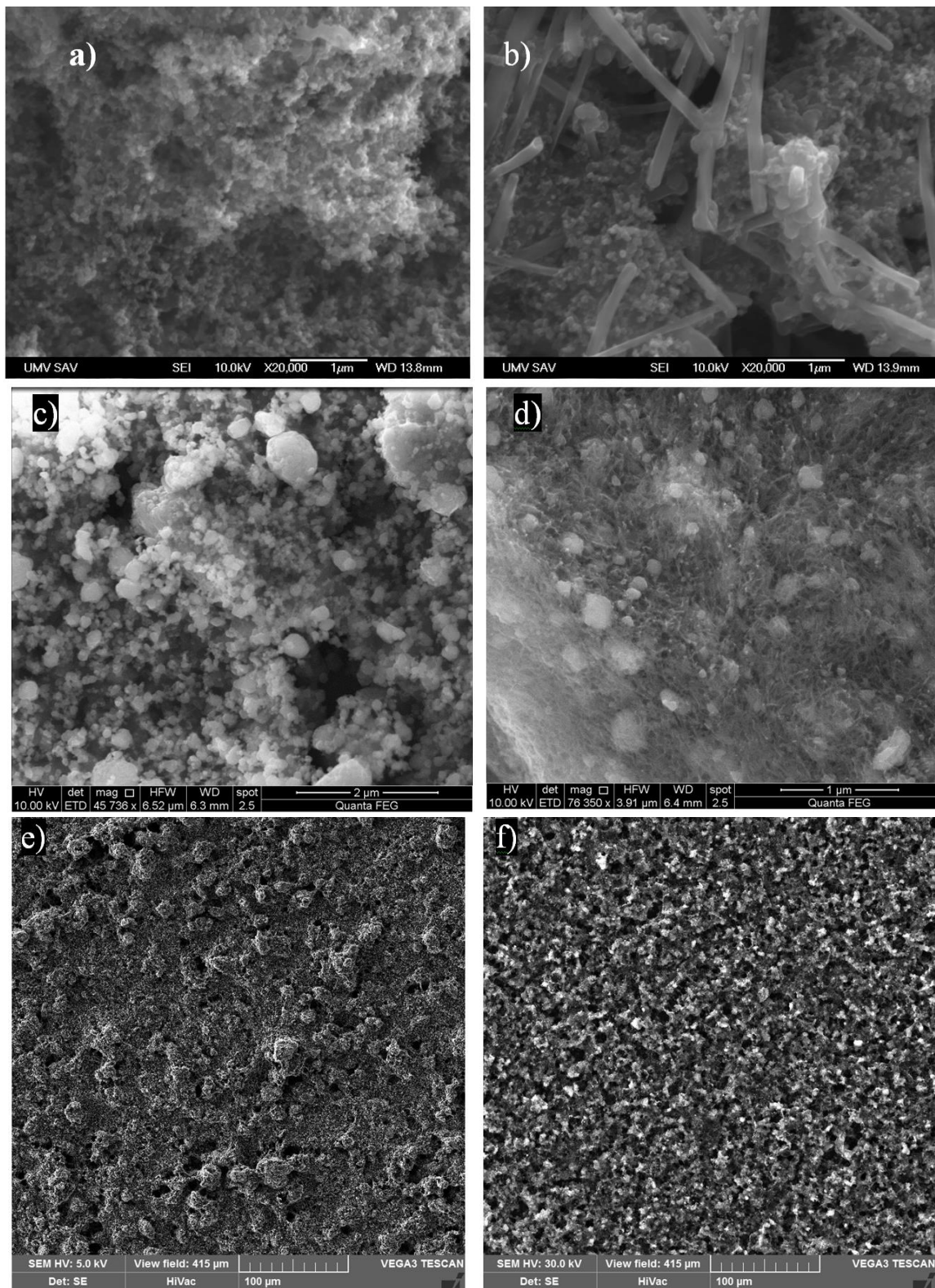


**Figure 1.** SEM images showing the morphology of sulfur-carbon (a), sulfur-carbon-MWCNTs (b), sulfur-LFP (c), S-LFP-MWCNTs (d), S-C-MWCNTs slurry coated on Al foil (e) and S-LFP-MWCNTs slurry coated on Al foil (f).

Rougher structure of the S-LFP (Figure 1c) cathodes (in comparison with S-C sample) was observed by SEM microscopy. Sample containing S-LFP-MWCNTs composite (Figure 1d) presents a more homogeneous structure with aligned fibres of MWCNTs on the surface.

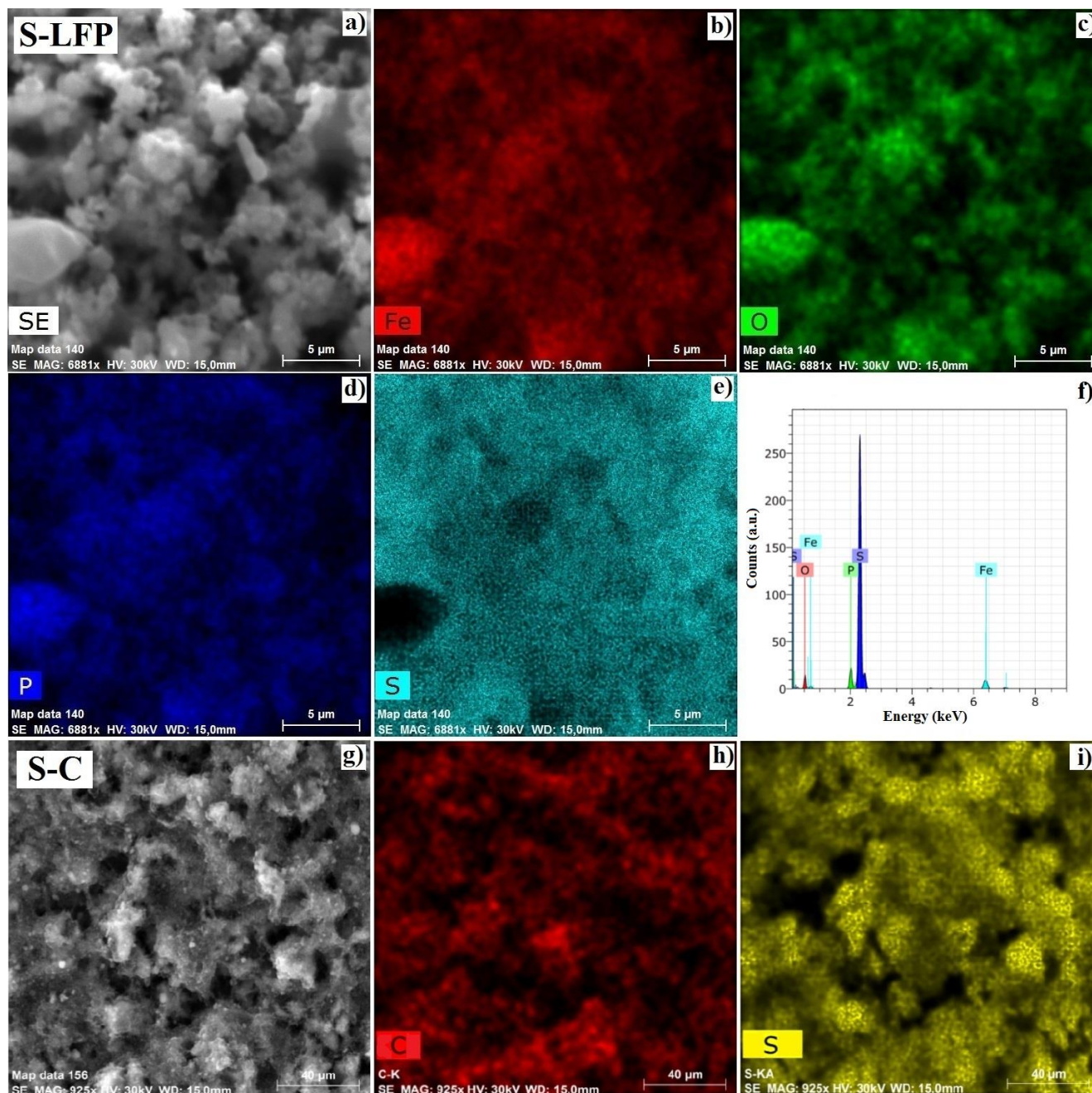


**Figure 2.** SEM images of S-LFP-MWCNTs (a-e) and S-C-MWCNTs (g-i) samples coated on Al foil with corresponding elemental maps captured for the selected region and EDX spectrum for S-LFP-MWCNTs sample (f).

Images obtained by SEM microscopy confirmed that the presence of MWCNTs in both samples can cause a significant change in porosity and homogeneity. SEM images of sulfur composites coated on Al foil are shown in Figures 1e,f. The coatings of S-C-MWCNTs (e) and S-LFP-MWCNTs

(f) are well adhered without any breakage or holes. The LFP composite cathode (f) showed the more porous structure. No large bulk particles can be easily observed, suggesting that the sulfur, carbon, LFP and MWCNTs are uniformly embedded in the cathode structure. This porous structure could be expected to be beneficial for a proper electrolyte impregnation, shortening the path for  $\text{Li}^+$  ion and electronic transport, and leading to a superior rate cycling performance. For further testing we chose only samples containing MWCNTs.

To confirm the composition of our samples energy dispersive X-ray spectroscopic (EDX) characterization and elemental mapping were carried out. EDX map analysis (Fig. 2) proved that the sulfur is uniformly distributed throughout both samples. Our findings are highly in agreement with the SEM results and it is clear that sulfur has been homogeneously embedded into the pores of carbon and LFP particles. EDX map analysis (Fig. 2) proved that the sulfur is uniformly distributed throughout both samples. Our findings are highly in agreement with the SEM results and it is clear that sulfur has been homogeneously embedded into the pores of carbon and LFP particles.

The thermogravimetric analysis (TGA and DTA) results for sulfur composites are shown in Fig. 3. Thermal stability measurements of S-C material in Ar atmosphere show one major weight loss in the thermogram and also in the differential thermal analysis (TGA-DTA) curves, as shown in Fig. 3a. That weight loss, taking place between 130–300 °C corresponds to sulfur vaporization, and amounts to ca. 48 wt %. A previous study on the TGA analysis of a sulfur-conducting material composite suggested that a weight loss detected between ca. 160–280 °C was mainly due to the evaporation of sulfur [11,21]. Fig. 3b shows the TGA results collected for the S-LFP-MWCNTs composite and also for pure sulfur and  $\text{LiFePO}_4$ . The mass loss of the S-LFP-MWCNTs composite starts at 170 °C and is continually decreasing up to 460 °C. The sulfur content was estimated at ca. 62 % in the S-LFP-MWCNTs composite. The weight change of both samples with sulfur has same trend and it can be clearly observed that sulfur was evaporated in temperature range 170-500 °C as shown in Fig. 3b.

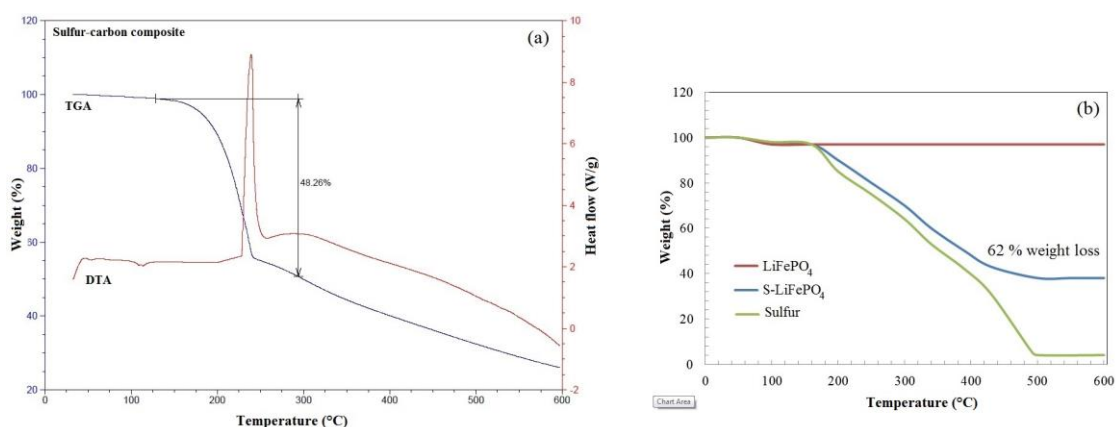


**Figure 3.** TGA and DTA curve of the sulfur-carbon composite (a) and TGA curves of pure sulfur, pure LFP and S-LFP composite (b).

3D-FTIR spectra were used to record the decomposition process. This process is very important to predict the fire safety of materials used in batteries with high energy density. The three

axes represent the wavenumber, absorbance units and time of the process, respectively (Fig. 4). The 3D-FTIR spectra of S-C-MWCNTs and S-LFP-MWCNTs samples show that the decomposition products corresponding to the peaks are very similar, indicating only evolved gases consisting of sulfur and carbon. As shown in Fig. 4a,b, the samples started to produce gases at *ca.* 200 - 220 °C (40 min, starting temperature 25 °C), generating a massive amount of SO<sub>2</sub> and CO<sub>2</sub> gasses. The absorption peaks at 2359 and 669 cm<sup>-1</sup> correspond to the evolution of carbon dioxide. SO<sub>2</sub> shows a small peak at 1100 cm<sup>-1</sup> and very strong peak at 1300–1400 cm<sup>-1</sup> region. Due to the higher amount of sulfur in S-LFP-MWCNTs sample we noticed that the absorption intensity is higher in comparison with S-C-MWCNTs sample (Fig. 4b). However evolution of CO<sub>2</sub> gas from S-C-MWCNTs sample gradually increased from 220 °C to 340 °C and remain constant up to 560 °C (Fig. 4a). The above results show a strong thermal and chemical stability of both sulfur based samples. These results also confirmed that no dangerous gaseous products were detected during the thermal decomposition of tested samples. Hence we can conclude that sulfur based composite samples are safe also at higher temperatures.

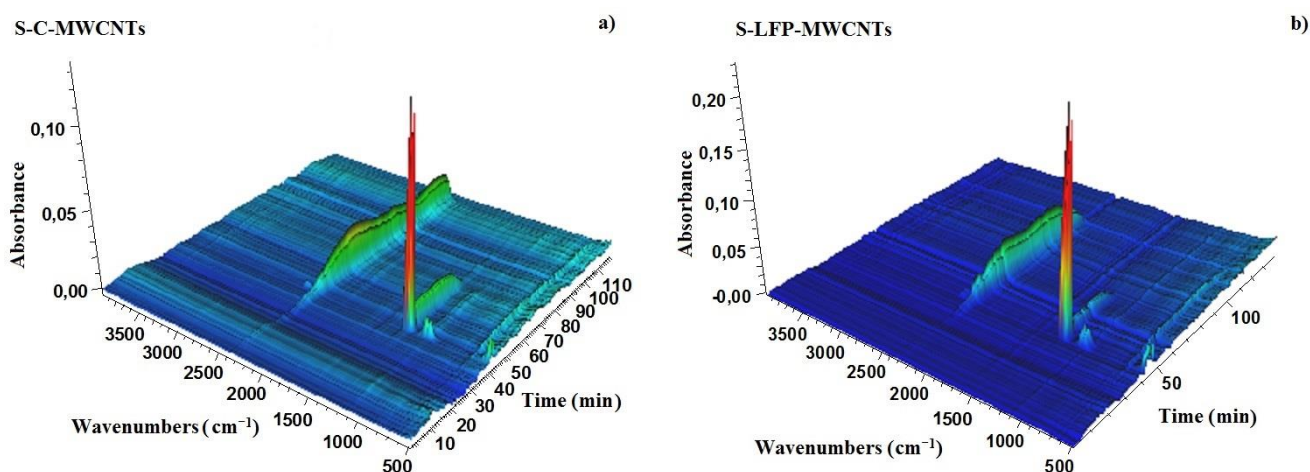


**Figure 4.** 3D-FTIR spectra of the evolved gaseous products of (a) S-C-MWCNTs and (b) S-LFP-MWCNTs sample at a heating rate of 5 °C/min.

The surface chemical composition and of the samples was investigated also by X-ray photoelectron spectroscopy (XPS), as shown in Fig. 5. The survey XPS spectrum (Fig. 5a) of the S-C-MWCNTs and S-LFP-MWCNTs composites confirms the presence of sulfur which is in agreement with our previous results. The binding energies (BE) of O 2s, S 2p, S 2s, C 1s and O 1s, were determined to be 28.10 eV, 165.08 eV, 230.20 eV, 286.10 eV and 538.20 eV respectively. The S 2p spectra (Fig. 5b) of the S-LFP-MWCNTs sample can be divided into three peaks. The peaks of 163.90 eV and 165.08 eV may be contributed by the S 2p<sub>3/2</sub> and S 2p<sub>1/2</sub> sulfur species confirming S-S bond in low chain S<sub>x</sub> (x≤8). Peak with binding energy 168.28 eV is related to the sulfate species. The binding energy of the S 2p<sub>3/2</sub> peak (163.9 eV) is lower than that of elemental sulfur (164.0 eV) [22, 23] which can confirm creation of bonds between atoms of sulfur and carbon during the solid state reaction in ball mill. Absence of Fe and P peaks confirmed that the LFP particles are homogeneously covered by sulfur (analysis depth max 5-10 nm).

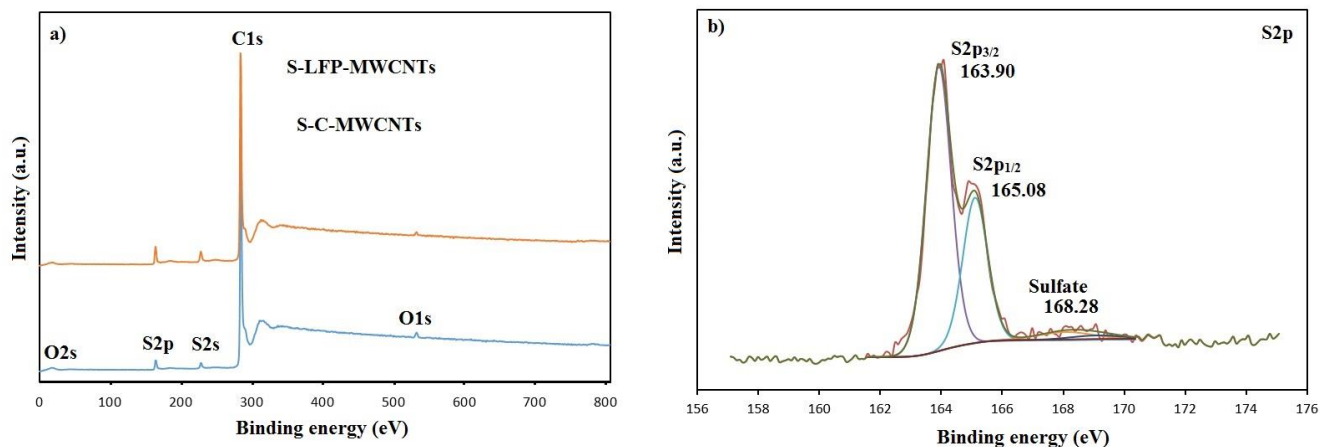


**Figure 5.** XPS spectra of the surface chemical composition of S-C-MWCNTs and S-LFP-MWCNTs samples (a), S2p XPS spectrum of the S-LFP-MWCNTs sample (b).

The charge/discharge curves of the sulfur based electrodes with and without LFP for the 1<sup>st</sup> and 2<sup>nd</sup> cycle at a C-rate 0.1 C are depicted in Fig. 6. Electrode material consisting of S-C sample (Fig. 6a) after assembling the testing cell was in charged state and therefore we can observe shorter charging cycle. During the first two cycles formation of the electrode is running what was confirmed by electrochemical charge/discharge measurements. Two discharge plateaus are observed in the discharge profiles of both samples (plateau 1. and plateau 2.). The same behavior was found also in charge profile (plateau 3. and plateau 4.) of the sulfur–carbon composite cathode. Two plateaus were observed also for S-LFP composite cathode (Fig. 6b). The gap potential between the charge and discharge plateaus for sample containing LFP is reduced, suggesting the smaller polarization and thus the faster kinetics of electrochemical reaction. This result confirmed that sulfur was adequately confined to carbon/MWCNTs matrix which provides protection against the polysulfides diffusion.

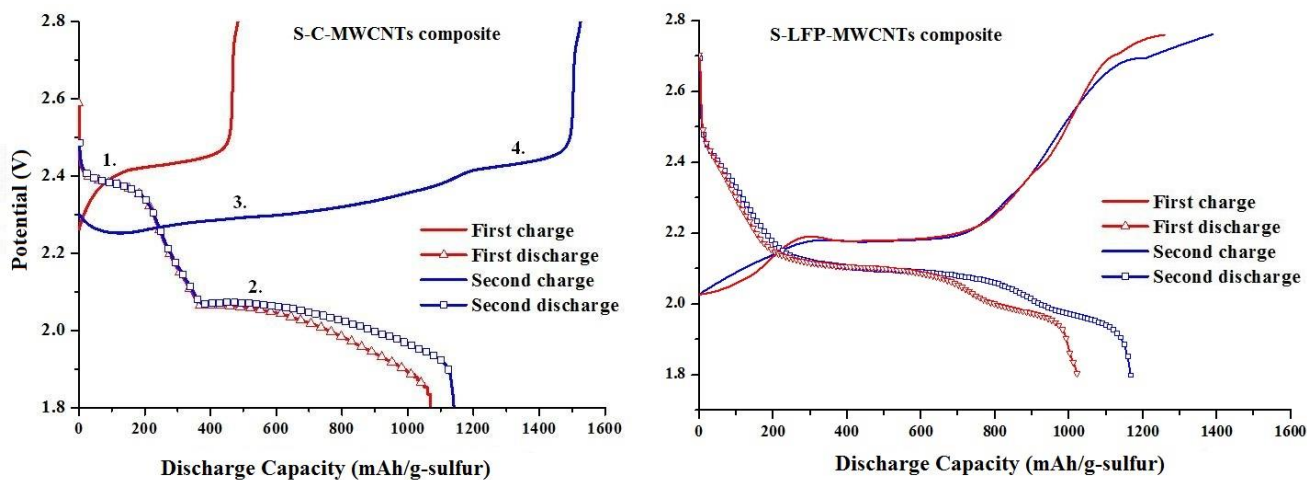


**Figure 6.** First two charge and discharge cycles of sulfur-carbon composite cathode (a) and sulfur-LFP cathode (b) at C-rate C/10.

Initial discharge capacity measured for S-C-MWCNTs sample was 1140 mAh/g-sulfur and for S-LFP-MWCNTs sample it was 1167 mAh/g-sulfur. These values correspond to 67% and 70% of the theoretical capacity of the sulfur. Our calculations based on the discharge capacity confirmed that at least 1.4 electrons per sulfur atom were involved in the electrochemical reactions of the S-LFP composite. Both electrodes (Fig. 6a,b) show two discharge and two charge plateaus, which is in accordance with CV curves (Fig. 8a).

The rate performance of sulfur composite samples are shown in Fig. 7. Figure 7a shows a discharge capacity of S-C-MWCNTs and S-LFP-MWCNTs samples at a scan rate 0.1C. The discharge capacity of S-C-MWCNTs sample and S-LFP-MWCNTs is 1180 and 1160 mAh/g-sulfur respectively, and retains 980 and 780 mAh/g-sulfur after 20 cycles. LFP containing cathode delivered a stabilized specific capacity of 980 mAh/g-sulfur a 20 % higher than that of S-C-MWCNT (780 mAh/g-sulfur). This behaviour can be assigned to  $\text{LiFePO}_4$  additive which can stabilize the polysulfide adsorption reaction, lowers the polarization for oxidation of  $\text{Li}_2\text{S}_2/\text{Li}_2\text{S}$  and contribute to the cell capacity at low current as was confirmed by Kim et al. [24]. Moreover, it is necessary to notice that a stable passivation film created by  $\text{LiNO}_3$  addition can improve electrochemical performance of sulfur cathodes [25].

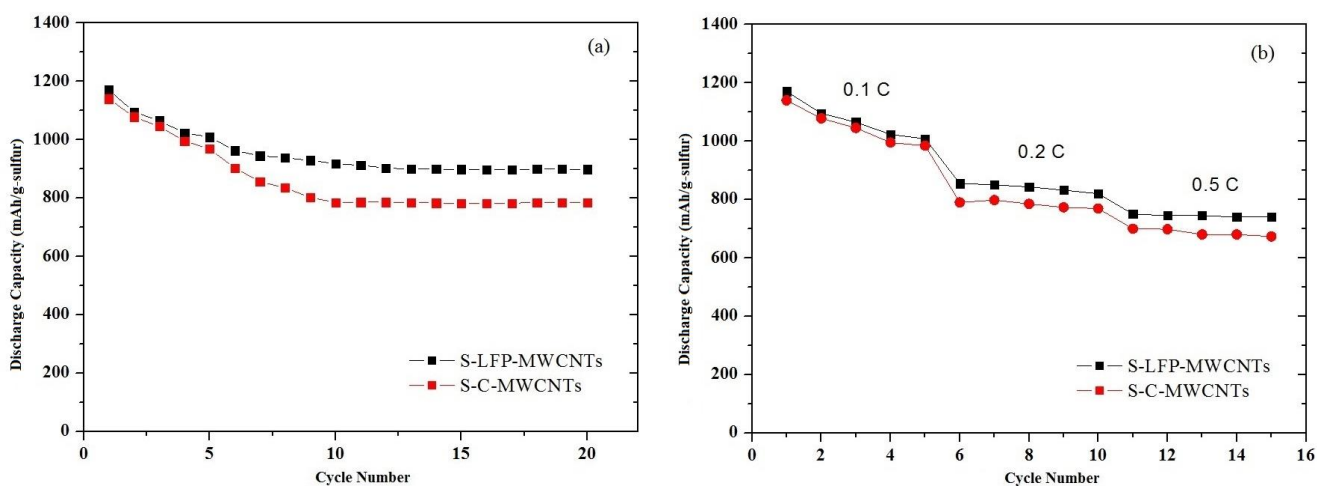


**Figure 7.** Cycling performance measured on S-C-MWCNTs and S-LFP-MWCNTs cathodes at a C-rate C/10 (a), rate performance of S-C-MWCNTs and S-LFP-MWCNTs cathodes at various C-rates (b).

The discharge capacity constantly decreases as the current rate is raised from 0.1 C to 0.5 C for both of the cells (Fig. 7b). The highest discharge capacities of 1170, 855 and 750 mAh/g-sulfur were achieved at a current density of 0.1, 0.2, and 0.5 C, respectively for S-LFP composite material.

Fig. 8a shows the cyclic voltammograms (CV) of S-C-MWCNTs and S-LFP-MWCNTs samples. Two cathodic peaks are observed at potentials 2.31 V and 1.99 V during the first cycle. The first cathodic peak at 2.31 V corresponds to the transformation from elemental sulfur to long chain polysulfides ( $\text{Li}_2\text{S}_n$ ,  $4 < n < 8$ ) [26]. The second cathodic peak at 1.99 V is associated to the reduction of higher-order polysulfides to  $\text{Li}_2\text{S}_2$  and  $\text{Li}_2\text{S}$ . The oxidation reaction from polysulfides back to the sulfur also result in two stages. The first oxidation peak at 2.4 V corresponds to the production of

$\text{Li}_2\text{S}_n$  ( $n > 2$ ), which is oxidized to elemental sulfur at 2.49 V. In case of both samples the peak positions and the peak currents change only slightly.

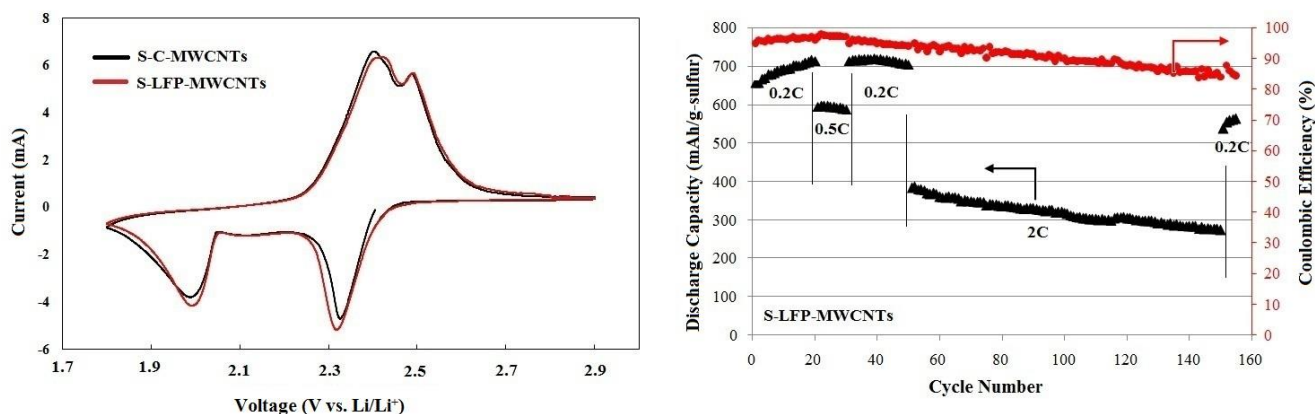


**Figure 8.** The cyclic voltammograms of S-C-MWCNTs and S-LFP-MWCNTs sample, scan rate 0.2 mV/s (a), long-term galvanostatic cycling of S-LFP-MWCNTs sample at various C-rates.

For further investigation of the electrochemical properties, galvanostatic long term cycling was performed with S-LFP-MWCNTs sample (Fig. 8b). The S-LFP-MWCNTs cathode can achieve the highest initial discharge capacity of 719, 595 and 384 mAh/g-sulfur at rates of 0.2 C, 0.5 C, and 2 C, respectively. After 160 charge/discharge tests, the cathode displays a stable capacity of 561 mAh/g-sulfur at the C-rate of 0.2 C. The average Coulombic efficiency with different rates is gained around the level of 91.5% during the 160 cycles. The improved electron and Li-ion diffusion during the charge/discharge process could be attributed to combination of sulfur and  $\text{LiFePO}_4$  cathode material [27].

#### 4. CONCLUSIONS

In summary, we have successfully synthesised sulfur composite cathodes using a simple, low-cost and environmentally friendly procedure. SEM micrographs confirmed that our samples based on sulfur (S-C-MWCNTs and S-LFP-MWCNTs) shows high porosity and homogeneity. The sulfur content in S-LFP-MWCNTs composite determined by TGA measurements was 62 wt. %. Initial discharge capacity measured for S-C-MWCNTs sample was 1140 mAh/g-sulfur and 1167 mAh/g-sulfur for S-LFP-MWCNTs sample. Charge/discharge measurements of S-LFP-MWCNTs sample confirmed smaller polarization and thus the faster kinetics of electrochemical reaction. After 160 charge/discharge tests, the cathode displays a stable capacity of 561 mAh/g-sulfur at the a C-rate of 0.2 C. MWCNTs and LFP additive can decrease solubility of higher polysulfides due to increased porosity of final cathode. Improved electrochemical performance can be attributed to the synergy between sulfur, LFP and MWCNTs components. Improved safety of sulfur composite samples was confirmed by 3-D FTIR spectroscopy measurements where only  $\text{SO}_2$  and  $\text{CO}_2$  gaseous products were detected.

All results described in this study indicate that the combination of sulphur, LiFePO<sub>4</sub> and MWCNTs is a promising cathode material for high-performance lithium-sulfur batteries.

#### ACKNOWLEDGEMENT

This research was sponsored by the NATO Science for Peace and Security Programme under grant 985148 and by the project VEGA 1/0074/17.

#### References

1. P.G. Bruce, S.A. Freunberger, L.J. Hardwick, J.M. Tarascon, *Nat. Mater.*, 11 (2012) 19-29.
2. X. Ji, L.F. Nazar, *J. Mater. Chem.*, 20 (2010) 9821-9826.
3. X. Tao, J. Wang, L. Chong, H. Wang, H. Yao, G. Zheng, W.S. Zhi, Q. Cai, W. Li, G. Zhou, *Nat. Commun.*, 7 (2016) 1-9.
4. R.V. Bugga, S.C. Jones, J. Pasalic, C.S. Seu, J.-P. Jones, L. Torres, *J. Electrochem. Soc.*, 164 (2) (2017) A265-A276.
5. Y. Ma, H. Zhang, B. Wu, M. Wang, X. Li, H. Zhang, *Sci Rep.*, 5 (2015) 14949.
6. M. Agostini, S. Xiong, A. Matic, J. Hassoun, *Chem. Mater.*, 27 (2015) 4604-4611.
7. C. Wang, J. Chen, Y. Shi, M. Zheng, Q. Dong, *Electrochim. Acta*, 55 (2010) 7010-7015.
8. J. Liang, Z.H. Sun, F. Li, H.M. Cheng, *Energy Storage Mater.*, 2 (2016) 76-106.
9. P. Pórolniczak, P. Nowicki, K. Wasinski, R. Pietrzak, M. Walkowiak, *Solid State Ionics*, 297 (2016) 59-63.
10. W. Wei, J. Wang, L. Zhou, J. Yang, B. Schumann, Y. NuLi, *Electrochem. Comm.*, 13 (2011) 399-402.
11. H. Wang, Y. Yang, Y. Liang, J.T. Robinson, Y. Li, A. Jackson, Y. Cui, H. Dai, *Nano Lett.*, 11 (2011) 2644-2647.
12. B. Zhang, X. Qin, G.R. Li, X.P. Gao, *Energy Environ. Sci.*, 3 (2010) 1531-1537.
13. J. Guo, Y. Xu, C. Wang, *Nano Lett.*, 11 (2011) 4288-4294.
14. J. Wang, J. Chen, K. Konstantinov, L. Zhao, S.H. Ng, G.X. Wang, Z.P. Guo, H.K. Liu, *Electrochim. Acta*, 51 (2006) 4634-4638.
15. A. Fedorkova, A. Nacher-Alejos, P. Gómez-Romero, R. Orinakova, D. Kaniansky, *Electrochim. Acta*, 55 (2010) 943-947.
16. J.L. Wang, J. Yang, J.Y. Xie, N.X. Xu, Y. Li, *Electrochem. Commun.*, 4 (2002) 499-502.
17. L.X. Yuan, H.P. Yuan, X.P. Qiu, L.Q. Chen, W.T. Zhu, *J. Power Sources*, 189 (2009) 1141-1146.
18. P. Xin, B. Jin, H. Li, X. Lang, C. Yang, W. Gao, Y. Zhu, W. Zhang, S. Dou, Q. Jiang, *ChemElectroChem*, 4 (2017) 115-121.
19. F. Yin, X. Liu, Y. Zhang, Y. Zhao, A. Menbayeva, Z. Bakenov, X. Wang, *Solid State Sci.*, 66 (2017) 44-49.
20. X. Liang, Y. Liu, Z.Y. Wen, L.Z. Huang, X.Y. Wang, H. Zhang, *J. Power Sources*, 196 (2011) 6951-6955.
21. M. Rao, X. Song, H. Liao, E.J. Cairns, *Electrochim. Acta*, 65 (2012) 228-233.
22. K.A. See, Y.-S. Jun, J.A. Gerbec, J.K. Sprafke, F. Wudl, G.D. Stucky, R. Seshadri, *ACS Appl. Mater. Interfaces*, 6 (2014) 10908-10916.
23. S. Zheng, P. Han, Z. Han, H. Zhang, Z. Tang, J. Yang, *Sci. Rep.*, 4 (2014) 4842.
24. C.-S. Kim, A. Guerfi, P. Hovington, J. Trottier, C. Gagnon, F. Barray, A. Vijh, M. Armand, K. Zaghib, *Electrochem. Comm.*, 32 (2013) 35-38.
25. J. Xu, B. Jin, H. Li, Q. Jiang, *Int. J. Hydrogen Energy*, 42 (2017) 20749-20758.
26. Y.-J. Li, J.-M. Fan, M.-S. Zheng, Q.-F. Dong, *Energy Environ. Sci.*, 9 (2016) 1998-2004.

27. D. Xu, P. Wang, B. Shen, *Ceram. Int.*, 42 (2016) 5331–5338.

© 2018 The Authors. Published by ESG ([www.electrochemsci.org](http://www.electrochemsci.org)). This article is an open access article distributed under the terms and conditions of the Creative Commons Attribution license (<http://creativecommons.org/licenses/by/4.0/>).